Mechanical–electrochemical coupling theory of bacterial cells

Huanxin Zhang [a], Huabin Wang [b,c,d,*], Yuan Gao [a], Kaixuan Zhang [a], Dominic Vella [e], and Xi-Qiao Feng [a,*]

[a] *Institute of Biomechanics and Medical Engineering, AML, Department of Engineering Mechanics, Tsinghua University, Beijing 100084, China*

[b] *Research Center of Super-Resolution Optics, Chongqing Institute of Green and Intelligent Technology, Chinese Academy of Sciences, Chongqing 400714, China*

[c] *Chongqing School, University of Chinese Academy of Sciences, Chongqing 400714, China*

[d] *Chongqing Engineering Research Center of High-Resolution and Three-Dimensional Dynamic Imaging Technology, Chongqing 400714, China*

[e] *Mathematical Institute, University of Oxford, Woodstock Rd, Oxford, OX2 6GG, UK*

[*] Corresponding authors.

E-mail addresses: wanghuabin@cigit.ca.cn (H. B. Wang) and fengxq@tsinghua.edu.cn (X. Q. Feng).

Abstract

The environmental adaption, growth, motion, and other dynamic behaviors of bacteria are closely associated with the coupled mechanical–electrochemical properties of their subcellular structures, but the underlying regulatory mechanisms remain unclear. The mechanical responses of bacteria are difficult to be elucidated by the traditional models without considering the mechanical, chemical, and electric coupling effects. In this paper, a mechanical–electrochemical theory is constructed to investigate the deformation behaviors of bacterial cells. A bacterium is treated as a bilayer structure consisting of a negatively charged polysaccharide capsule and an elastic envelope subjected to the turgor pressure. This model is used to reveal the regulating roles of the electrostatic double-layer force and osmosis under different electrolyte conditions. A good agreement is found between the theoretical predictions and the experimentally observed three-stage nanoindentation responses of *Klebsiella pneumoniae* bacterial cells. Furthermore, we investigate the mechanical–electrochemical coupling mechanisms in the compression resistance of the bacterial capsule. The results reveal that the osmosis induced by ionic imbalance and polysaccharide–solvent aggregates plays a significant role in the compression resistance of the capsule. The present model can not only deepen our understanding of the mechanical–electrochemical coupling mechanisms of bacterial cells at the subcellular scale, but also holds promise for applications in characterizing their mechanical properties.

Keywords: Bacteria; Mechanical–electrochemical coupling; Nanoindentation; Osmosis; Electrostatic double-layer force

1. Introduction

Bacteria have strong adaptabilities to complex physiological environments, such as temperature, osmosis, light, and antibiotics (Ohyama et al., 1992; Pilizota and Shaevitz, 2012; Rojas et al., 2014). The mechanical properties of bacterial cells are crucial in their adaptabilities and dynamic behaviors, e.g., growth, division, and motion (Jiang and Sun, 2010; Liu et al., 2020; Monteiro et al., 2015). The capsular electrochemistry, envelope elasticity, and cytoplasmic turgor pressure are strongly coupled in the mechanical responses of bacteria to external stimuli. The turgor pressure stems from the osmotic difference between the cytoplasm and extracellular environment, and points toward the cell envelope. The capsule on the bacterial surface primarily consists of a polysaccharide molecule (PM) network, which carries negative charges and imbibes water (Gaboriaud et al., 2008; Moxon and Kroll, 1990; Vadillo-Rodriguez et al., 2004). The negatively charged and hydrated polymeric network determines the compression resistance of the capsule (Mei et al., 2006), thus having a remarkable influence on the overall mechanical properties of a cell when subjected to external loads. The cell envelope, which is remarkably stiff and confers a high tensile strength of bacteria cells, maintains the integrity of cell morphology (Arnoldi et al., 2000; Boulbitch et al., 2000; Deng et al., 2011). Both the polysaccharide capsule and the cell envelope pose physical barriers to the external environment. To construct a mechanical model of bacterial cells, we need to consider not only the coupling mechanism among the mechanical–electrochemical cues but also their layered structures consisting of a negatively charged polysaccharide capsule and an elastic envelope.

Considerable experimental and theoretical efforts have been directed toward revealing the contributions of mechanics and electrochemistry of subcellular structures to the overall properties of bacteria (Gaboriaud et al., 2008; Mei et al., 2006; Phanphak et al., 2019; Wang et al., 2013). Atomic force microscope (AFM) provides a powerful tool to investigate the elasticity, viscoelasticity, and electrostatic interaction of

individual bacterial cells at the nanoscale level and under various (near-) physiological conditions (Camesano and Logan, 2000; Pelling et al., 2005). Previous theoretical studies have treated the polysaccharide capsule as a brush-like structure and used the Pincus theory to describe the compression resistance, which is mainly determined by the polymer density of the polyelectrolyte brush layer (Abraham et al., 2000; Considine et al., 2001; Wang et al., 2013). However, these previous models are difficult to account for the electrochemical behavior of the capsule. Although the Derjaguin–Landau–Verwey–Overbeek (DLVO) theory considers the adhesion, electrostatic, and van der Waals interaction of the charge-regulated bacterial cell surface (Gaboriaud et al., 2008; Hwang et al., 2012), it is hard to be used to treat the electrochemical and mechanical properties of the capsule, which involve the changes in the external osmosis, ionic concentration, and deformation. Hitherto, it remains elusive how these mechanical–electrochemical mechanisms and subcellular structures coherently affect the mechanical properties of bacterial cells.

In this paper, we propose a coupled mechanical–electrochemical model consisting of a negatively charged capsule and an elastic envelope to rationalize the contributions of mechanical and electrochemical properties. Compared with previous theoretical studies of bacterial cells (Arnoldi et al., 2000; Deng et al., 2011), we model a bacterial cell as a bilayer capsule–envelope structure subjected to a turgor pressure, decoding the regulating roles of subcellular mechanical–electrochemical features in its deformation behavior. The polysaccharide capsule is modeled as a charged polymer gel, and the stiff cell envelope is considered as a linear elastic material. To verify this model, the mechanical properties of *Klebsiella pneumoniae* bacteria are probed by AFM nanoindentation. The theoretical predictions agree well with the experimental results. We also find that the osmosis originating from ionic imbalance and polysaccharide–solvent aggregates determines the mechanical resistance of the capsule, which can help elucidate why the mechanical behaviors of bacteria are sensitive to the electrolyte concentration.

This paper is organized as follows. Section 2 presents a finite-deformation mechanical–electrochemical coupling theory of live bacterial cells. In Section 3, the mechanical properties of *K. pneumonia* bacteria in hypotonic and hypertonic aqueous environments are characterized by AFM-based nanoindentation tests. In Section 4, the theory is applied to analyze the nanomechanical behaviors and compression resistance of a polysaccharide capsule. Finally, we summarize the main conclusions drawn from this study.

2. Theory

2.1. Layered structure of a bacterial cell

A bacterial cell, such as *Escherichia coli*, *K. pneumonia*, and *Bacillus subtilis*, has a multi-layered structure, mainly consisting of a polysaccharide capsule, a cell envelope, and a fluidic cytoplasm, which have greatly different mechanical properties, as shown in Fig. 1(a). The responses of a bacterium to external stimuli involve the complicated coupling of mechanical, chemical, and electric fields in its solid and liquid phases. In this work, we integrate these coupled mechanisms of multiple subcellular structures in the framework of continuum mechanics. The deformation of a bacterium subjected to external stimuli is considered as an isothermal process at the physiological condition. In the outer layer, the polysaccharide capsule with the PM network is treated as a solid skeleton that ensures the structural and mechanical integrity of the cell, and the interstitial space is filled with fluid, consisting of water and solutes (e.g., chemical factors and oxygen). Thus, we will use the theory of the charged polymeric gel to model the polysaccharide capsule. The cell envelope is simplified as a linear elastic cylindrical shell with two hemi-spherical caps (Vella et al., 2012a, b). The cytoplasm, which is filled with cytosol and organelles, provides a turgor pressure (p) acting on the cell envelope. The dielectric polarization of the capsule will be incorporated into the finite deformation theory to describe surface intermolecular interactions. Thus, the bacterium is regared as a bilayered solid structure consisting of a negatively charged

polysaccharide capsule and a cell envelope subjected to the internal turgor pressure, as shown in Fig. 1(b).

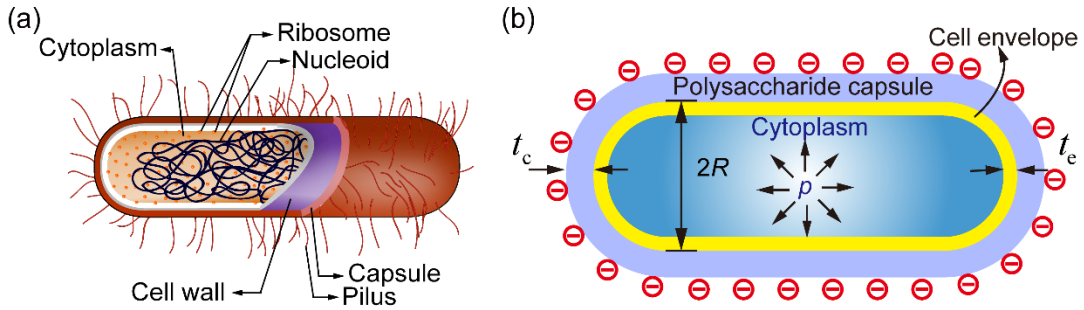

Fig. 1. (a) Schematics of the multi-layered structure of a bacterial cell. (b) A bilayer capsule–envelope model, including a negatively charged capsule of thickness t_c and a cell envelope of thickness t_e subjected to the cytoplasm pressure p.

2.2. Model of polysaccharide capsule

In this work, the polysaccharide capsule is considered as a negatively charged polymeric gel containing a cross-linked PM polymer network as its solid skeleton (Fig. 1(b)). The capsule spacing in the network is filled with fluids consisting of the solvent (i.e., water) and solutes (e.g., ions and antibodies). The mechanical and electrochemical features of the swollen capsule under external stimuli can be characterized by using the hydrogel theory (Hong et al., 2009; Hong et al., 2010). It allows us to mathematically formulate the complicated interplay among the mechanical, chemical, and electric fields. Therefore, in contrast to such previous theories as the Pincus theory that describes the effects of mechanical properties and electrochemistry separately (Hwang et al., 2012; Wang et al., 2013), we consider the coupling mechanisms of these multiple fields, which play an essential role in the deformation behaviors of bacterial cells. For simplicity, we assume here that all states during the considered deformation process are quasi-static and approximately in equilibrium.

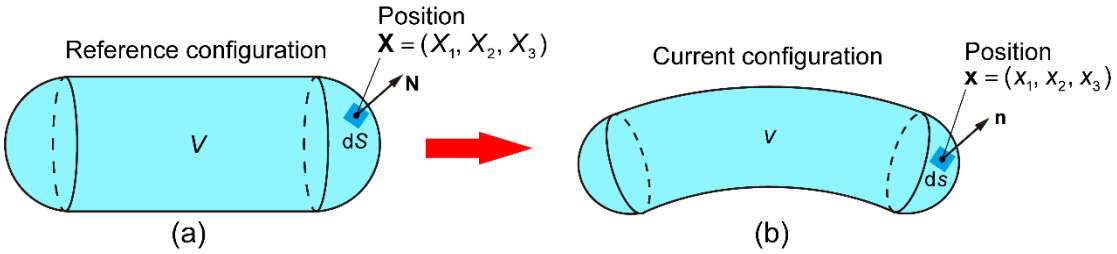

Fig. 2. Deformation of a polysaccharide capsule in (a) the stress-free reference configuration and (b) the current, deformed configuration.

The stress-free state of a polysaccharide capsule is defined as the reference configuration with total volume V, surface area S, and unit outward normal vector $\mathbf{N}$ at position $\mathbf{X}$. Upon loading, the capsule deformes from the reference state to the current configuration with total volume v, surface area s, and unit outward normal vector $\mathbf{n}$ at position $\mathbf{x}$, as shown in Fig. 2. Thus, the deformation gradient tensor is $\mathbf{F} = \partial\mathbf{x}/\partial\mathbf{X}$.

The PMs in the capsule are highly charged and hydrated (Stokes et al., 2011). Let $Q(\mathbf{X},t)$ denote the electric charge density per unit volume, including free electrons, ions, and fixed charges, that is,

$$Q = q + \sum_{\alpha} ez_{\alpha}C_{\alpha} + ez_0C_0, \tag{1}$$

where q is the electronic charge density per unit volume of the PM network, e denotes the elementary charge, z_{α} is the valence of the fluid phase α, and z_0 and C_0 are the valence and concentration of the fixed charges, respectively.

The dielectric polarization of the polymeric capsule can be described by Gauss's law of electrostatic fields (Suo et al., 2008). Accordingly, the nominal electric displacement $\hat{\mathbf{D}}(\mathbf{X},t)$ in the initial configuration satisfies

$$\nabla_R \cdot \hat{\mathbf{D}} = Q, \tag{2}$$

The deformation of a capsule involves the simultaneous evolutions of the solid PM network and the multiple fluid phases. Thus, the deformation gradient $\mathbf{F}$, the nominal concentration C_{α} of the fluid phase α, and the nominal electric displacement

$\hat{\mathbf{D}}$ are coupled. Let $w(\mathbf{F}, C_\alpha, \hat{\mathbf{D}})$ denote the Helmholtz free energy density per unit reference volume in the capsule. The constitutive equations of the polysaccharide capsule can be derived from the energy balance and dissipation inequality (Hong et al., 2010; Xue et al., 2017). The first Piola–Kirchhoff stress $\mathbf{P}$, the chemical potential μ_α of the α-th mobile species, and the electric potential Φ are given by

$$\mathbf{P} = \frac{\partial w}{\partial \mathbf{F}}, \tag{3}$$

$$\mu_\alpha = \frac{\partial w}{\partial C_\alpha} + e z_\alpha \Phi, \tag{4}$$

$$\nabla_R \Phi = -\frac{\partial w}{\partial \hat{\mathbf{D}}}, \tag{5}$$

respectively. Since the electric field is equal to the negative gradient of the potential, $\hat{\mathbf{E}}(\mathbf{X}, t) = -\nabla_R \Phi$, the nominal electric field can be calculated by

$$\hat{\mathbf{E}}(\mathbf{X}, t) = \frac{\partial w}{\partial \hat{\mathbf{D}}}. \tag{6}$$

In the capsule of a bacterial cell, PMs are entangled together, forming a PM network that provides the mechanical and structural integrity, imbibes the solution, and carries fixed negative charges (Hammerschmidt et al., 2005). We use a polymeric gel model to describe the prominent mechanical–electrical coupling features of the capsule immersed in different electrolyte solutions (Hong et al., 2009; Hong et al., 2010; Marcombe et al., 2010). Since PMs suspended in a solution of high dielectric constant are usually charged (Israelachvili, 2015; Wang et al., 2013), we consider the dielectric polarization following the Flory–Rehner theory. Thus, the Helmholtz free energy density of the capsule contains four main parts,

$$w = w_{\mathrm{n}} + w_{\mathrm{s}} + w_{\mathrm{i}} + w_{\mathrm{p}}, \tag{7}$$

where w_{n}, w_{s}, w_{i}, and w_{p} are the energies resulting from the deformation of the PM network, the mixing of the polymers and the solvent, the mixing of the solvent and ions, and the polarization of the capsule, respectively.

According to the Flory–Rehner theory (Flory, 1953), the capsule can be regarded

as an entropy elastomer, the free energy density induced by the PM network stretch can be expressed as

$$w_{\mathrm{n}} = \frac{1}{2} N k_{\mathrm{B}} T \left(\mathbf{F} : \mathbf{F} - 3 - 2 \ln J \right), \tag{8}$$

where N is the number of polysaccharide chains per unit volume in the dry network, and k_{B} is the Boltzmann constant. The conformational entropy of chains obeys the Gaussian statistics. The volume ratio induced by capsule swelling is usually very large, that is, $J >> 1$.

The free energy density induced by mixing the polysaccharide and the solvent is expressed as (Flory, 1942; Huggins, 1942)

$$w_{\mathrm{s}} = k_{\mathrm{B}} T C_{\mathrm{w}} \left(\ln \frac{C_{\mathrm{w}} v_{\mathrm{w}}}{1 + C_{\mathrm{w}} v_{\mathrm{w}}} + \frac{\zeta}{1 + C_{\mathrm{w}} v_{\mathrm{w}}} \right), \tag{9}$$

where C_{w} is the concentration of the solvent in the initial configuration, v_{w} the volume per solvent molecule, and ζ a dimensionless parameter characterizing the enthalpy of mixing, respectively. The free energy w_{s} is the contribution from the entropy and the enthalpy of mixing the PM and the solvent.

The free energy w_{i} induced by mixing the solvent (i.e., water molecules) and the solute ions depends on the entropy of mixing (Hong et al., 2010). It takes the form

$$w_{\mathrm{i}} = k_{\mathrm{B}} T \sum_{m} C_m \left(\ln \frac{C_m}{C_m^{\mathrm{ref}} C_{\mathrm{w}} v_{\mathrm{w}}} - 1 \right), \tag{10}$$

where C_m is the nominal concentration of the solute *m*, and C_m^{ref} is the reference concentration of the solute *m*.

According to Zhao et al. (2007), we assume that the capsule is an ideal dielectric elastomer with the free energy of polarization:

$$w_{\mathrm{p}} = \frac{1}{2\varepsilon} \mathbf{D} : \mathbf{D}, \tag{11}$$

where ε is the permittivity of the capsule, and $\mathbf{D}$ is the true electric displacement in the current configuration, and $\mathbf{D} = J^{-1} \mathbf{F} \cdot \hat{\mathbf{D}}$. The permittivity ε is estimated by the

volumetric average of the solvent and PM network:

$$\varepsilon = \frac{\varepsilon_{\mathrm{n}} + v_{\mathrm{w}} C_{\mathrm{w}} \varepsilon_{\mathrm{w}}}{1 + v_{\mathrm{w}} C_{\mathrm{w}}}, \tag{12}$$

where ε_{n} and ε_{w} are the permittivity of the network and solvent, respectively.

In general, the volume change of the PMs in the capsule is negligible in comparison with that induced by swelling. Thus the constraint condition can be given by

$$1 + \sum_{\alpha} C_{\alpha} v_{\alpha} = J, \tag{13}$$

where v_{α} is the volume per phase α.

Using the constraint condition in Eq. (13), the Helmholtz free energy density w can be recast as

$$w = w_{\mathrm{n}} + w_{\mathrm{s}} + w_{\mathrm{i}} + w_{\mathrm{p}} + \Lambda \left(1 + \sum_{\alpha} v_{\alpha} C_{\alpha} - J \right), \tag{14}$$

where Λ is the Lagrange multiplier. Λ can be interpreted as the overall fluid pressure in the capsule, expressed as $\Lambda = \Pi + p$, where Π is the osmotic pressure, and p is the fluid pressure in the external solution.

Substituting Eq. (14) into (3) and using Piola transformation, the Cauchy stress is derived as

$$\boldsymbol{\sigma} = J^{-1} \mathbf{F} \cdot \mathbf{P} = \frac{N k_{\mathrm{B}} T}{J} \left(\mathbf{F} \cdot \mathbf{F}^{\mathrm{T}} - \mathbf{I} \right) + \frac{1}{2\varepsilon} \left(2\mathbf{D} \cdot \mathbf{D}^{\mathrm{T}} - \mathbf{D}^{\mathrm{T}} \cdot \mathbf{D} \cdot \mathbf{I} \right) - \Lambda \mathbf{I}, \tag{15}$$

where the first term on the right-hand side is the contribution due to the network's entropy, and the second term is the Maxwell stress depicting the effect of the electric field on the deformation.

Substituting Eq. (14) into (4), the electrochemical potentials of the solvent and the solute m are obtained respectively as

$$\mu_{\mathrm{w}} = k_{\mathrm{B}} T \left[\ln \left(\frac{v_{\mathrm{w}} C_m}{1 + v_{\mathrm{w}} C_{\mathrm{w}}} \right) + \frac{1}{1 + v_{\mathrm{w}} C_{\mathrm{w}}} + \frac{\zeta}{\left(1 + v_{\mathrm{w}} C_{\mathrm{w}} \right)^2} - \sum_{m} \frac{C_m}{C_{\mathrm{w}}} \right] + \Lambda v_{\mathrm{w}}, \tag{16}$$

$$\mu_m = ez_m\Phi + k_{\mathrm{B}}T\ln\left(\frac{C_m}{\nu_{\mathrm{w}}C_{\mathrm{w}}C_m^{\mathrm{ref}}}\right) + \Lambda\nu_m . \tag{17}$$

Substituting Eqs. (14) into (6) and using Piola transformation, the true electric field in the current configuration (Zhao et al., 2007) is derived as

$$\mathbf{E} = \hat{\mathbf{E}}\cdot\mathbf{F}^{-1} = \frac{\mathbf{D}}{\varepsilon} . \tag{18}$$

2.3. Constitutive relation of cell envelope

In general, the bacterial envelope can be considered as a pressurized elastic shell subjected to a turgor pressure. Previous work has shown that the elastic modulus of the cell envelope is linearly related to the turgor pressure (Deng et al., 2011). Under a fixed internal pressure, the elastic modulus is regarded as a constant, as assumed in the previous work (Arnoldi et al., 2000; Vella et al., 2012a, b). Thus, the linear elastic model is adopted to describe the mechanical response of the cell envelope. Its constitutive relation is

$$\boldsymbol{\sigma} = \frac{E_{\mathrm{e}}}{1+\nu}\boldsymbol{\varepsilon} + \frac{E_{\mathrm{e}}\nu}{(1+\nu)(1-2\nu)}\left(\mathrm{tr}\boldsymbol{\varepsilon}\right)\mathbf{I} , \tag{19}$$

where E_{e} is the Young's modulus, ν the Poisson's ratio, and $\mathbf{I}$ the identity tensor.

2.4 Summary of the theoretical model

In summary, we have developed a mechanical–electrochemical coupling model to investigate the response of a bacterial cell to external stimuli. The cell is considered as a bilayer capsule–envelope structure subjected to the turgor pressure. The polysaccharide capsule layer is treated as a negatively charged polymeric gel with the coupling mechanisms of mechanical, chemical, and electric cues, as described by the constitutive relations in Eqs. (15)–(18). The cell envelope layer is treated as a linear elastic shell. Through the combination of the mechanical equilibrium equation and specific boundary conditions, we can solve the field variables of stresses, fluid chemical potentials, solute concentrations, and electric potentials. In what follows, this theory

will be used to analyze the nanoindentation tests and the compression resistance of a bacterial cell under different electrolyte conditions.

3. Nanoindentation tests of bacterial cells

K. pneumonia strain is a rod-shape Gram-negative pathogen that may cause a variety of hospital-acquired infections, e.g., surgical wound infections (Jenney et al., 2006). The subcellular structure of wild-type *K. pneumonia* is the same as that described in Section 2.2. We chose this strain as an example to explore the effects of osmosis and electrochemistry on the deformation of bacterial cells. A series of AFM nanoindentation tests of *K. pneumoniae* cells submerged in Milli-Q water and 100 mM $CaCl_2$ were conducted, as illustrated in Fig. 3(a). The two electrolyte solutions correspond to hypertonic and hypotonic conditions, respectively.

The radii of the bacterial cells were measured from the cross-sectional analysis of the AFM contact-mode three-dimensional height images (Zhang et al., 2021). The measurements show that the wild-type bacterial cells in Milli-Q water and 100 mM $CaCl_2$ have average radii of 352 ± 31 nm and 356 ± 38 nm, respectively, which have a small difference of only 1.8% (Wang et al., 2013). Previous experiments found that, after osmotic shock, the response of a bacterial cell relies on its mechanosensitive channels, which allow water and cytoplasmic solutes to pass across the cell membrane, helping to maintain the relative stability of the difference between the internal and external osmotic pressures, also termed as the turgor pressure. Through this mechanism, the volume of a bacterial cell can recover to its initial value in several minutes (Buda et al., 2016; Miermont et al., 2013). This indicates that bacterial cells have an adaptive ability to the variations in the external osmolarity.

It can be seen from our nanoindentation test results in Fig. 3(b) that, for a wild-type bacterial cell in Milli-Q water, the force–distance curve can be divided into three stages. First, Stage I appears before the AFM tip gets in contact with the cell. In the range of ~ 300 nm from the bacterial cell to the negatively charged silicon nitride AFM

tip, we can measure an increasing repulsive force. This confirms the previous electrohydrodynamic study that the polysaccharide capsule bears a certain amount of negative charges, which induce electrostatic interaction (Gaboriaud et al., 2008). Secondly, Stage II occurs after the tip has got in contact with and gradually compresses the surface polymer layer of the cell. In this stage, the indentation force–distance curve features a significant nonlinearity. This suggests that the polysaccharide capsule serves as a buffer to bear external stimuli, including the mechanical load and the electrolyte environment. As the indentation depth further increases, the tip presses the cell envelope and the force profile becomes approximately linear, with a much larger slope, which is referred to as Stage III. In this stage, the elastic deformation of the cell envelope plays a dominant role in the indentation response. The entire indentation process is schematically illustrated in Fig. 3(c).

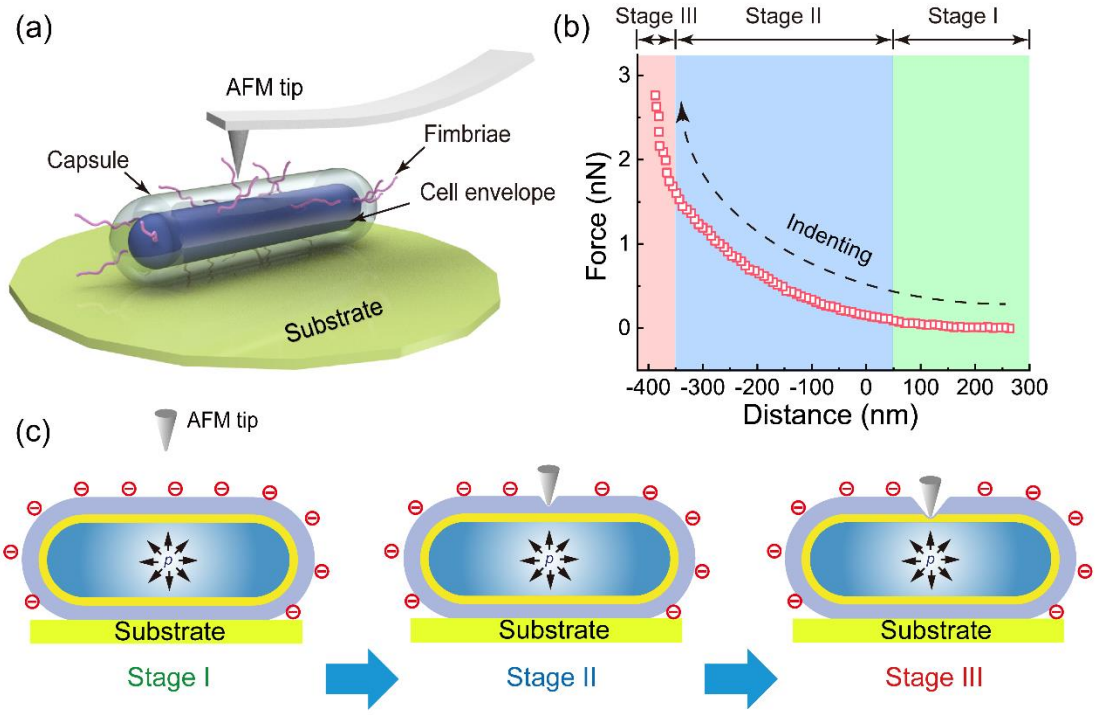

Fig. 3. Mechanical response of a wild-type *K. pneumoniae* cell under AFM indentation**.** (a) Schematic diagram of the indentation test of a bacterial cell with attached fimbriae adhered to a substrate. (b) An experimental nanoindentation force–distance curve of a wild-type (red squares) bacterial cell submerged in Milli-Q water. (c) Schematic

diagrams illustrating the mechanisms in the three stages of the nanoindentation response, in which the resistance of fimbria, also known as pilus, can be ignored due to its low density (Wang et al., 2013).

The indentation responses of a bacterial cell under two different osmotic conditions are compared in Fig. 4, which are closely associated with the influences of osmosis and electrochemistry on the cell deformation. Although the force–distance curves in Stage II and III of 100 mM $CaCl_2$ are similar to those in Milli-Q water, they have several differences as follows. First, for a wild-type bacterial cell in 100 mM $CaCl_2$, the electrostatic repulsive force is almost negligible in Stage I. This is because the negative charges on the PMs are neutralized by the Ca^{2+} ions in the solution. Second, the nonlinear Stage II of the cell in $CaCl_2$ is relatively shorter than that in Milli-Q water. This finding highlights the remarkable change in the structure of the polysaccharide capsule in response to the added electrolyte (Wang et al., 2013). In the following, we will use the mechanical-electrochemical coupling theory described in Section 2 to analyze the indentation behavior of *K. pneumoniae* cells and the compression resistance of the capsule under different conditions.

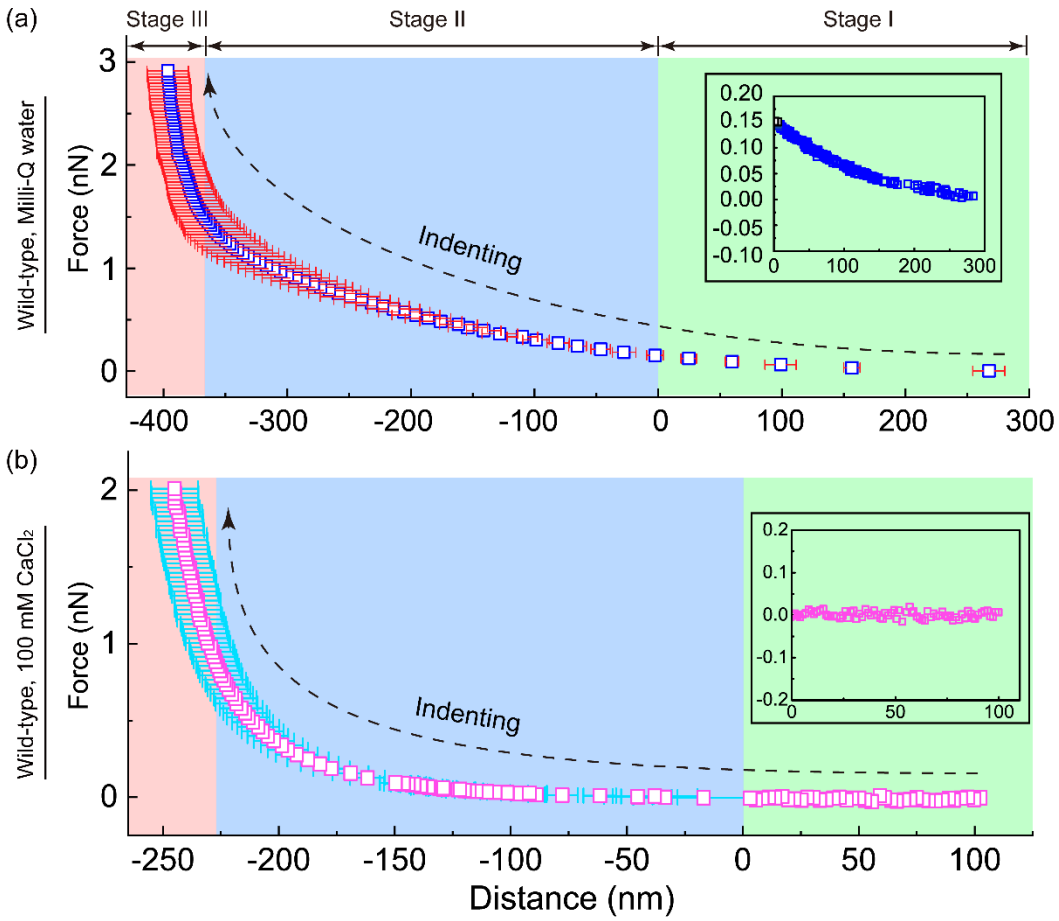

Fig. 4. Population-averaged indentation curves ($n \approx 200$ in each osmotic condition) of a wild-type cell in (a) Milli-Q water (blue squares) and (b) 100 mM $CaCl_2$ (pink squares). The red and cyan error bars represent the standard deviations under the two conditions. The long-range interaction between the wild-type cells and the AFM tip is shown in the insets of (a) and (b).

4. Theoretical validation and discussions

The above experimental results show that the indentation response of a bacterial cell can be divided into three stages, which stem from both its layered structures and their mechanical and electrochemical properties. In this section, we apply the mechanical–electrochemical coupling theory described in Section 2 to decode the underlying mechanisms of the three-stage nanoindentation response of a bacterial cell. The effect of external electrolytes on the compression resistance of the capsule will be examined to show the application of the theory. All parameters used in the present

model, and their resources, are listed in Table 1.

We first validate the mechanical-electrochemical coupling theory proposed in Section 2 by comparing it with the results of the experiments (Fig. 4) and finite element (FEM) simulations. To track the three-stage nanoindentation responses, we implement the proposed theory into the commercial software *Abaqus 6.14*. The approach of user-defined FEM simulation of the mechanical–electrochemical coupling model is given in Appendix I.

Table 1. Parameters used in the calculation.

Symbol	Description	Value	Source
k_B	Boltzmann constant	1.38×10^{-23} J	
T	Absolute temperature	298 K	
v_w	Volume of a water molecule	3×10^{-29} m^3	
ω_t	Surface charge density on AFM tip	–0.032 C m^{-2}	Mueller et al. (1999)
ζ	Dimensionless parameter of enthalpy of mixing	0.2	Xue et al. (2017)
z_0	Charge of a PM	–4	Xue et al. (2017)
C_0	Concentration of fixed charges	3.3×10^{25} m^{-3}	Gaboriaud et al. (2008)
t_e	Thickness of cell envelope	26 nm	Mularski et al. (2017)
R_t	Curvature radius of AFM tip	20 nm	Our experiments
θ	Cone angle of AFM tip	15°	Our experiments
ω_c	Surface charge density on the capsule in Milli-Q water	-2×10^{-4} C m^{-2}	Our experiments
N	Number density of polysaccharide chains	2.6×10^{23} m^{-3}	Our experiments
R	Bacterial radius	350 nm	Our experiments
p	Turgor pressure	80 kPa	Our experiments
E_e	Young's modulus of cell envelope	115 MPa	Our experiments

4.1. Electrostatic interaction

Due to the presence of negative charges on the capsule layer, an electrostatic repulsion occurs between the bacterial cell and the AFM tip. The electrostatic interaction plays an indispensable role in bacterial adhesion (Guo et al., 2018; Hayashi et al., 2001; James et al., 2017; Poortinga et al., 2002; Straub et al., 2019). In Stages II and III of the nanoindentation curve in Fig. 4, the electrostatic repulsive interaction force is much lower than the contact force, and thus the contribution of electrostatics to the deformation of the capsule is insignificant, as shown in Fig. 4(a). Therefore, the electrostatic interaction is not considered in the numerical model when simulating the indentation, instead, it is superimposed on the numerically obtained indentation force–depth curve. In what follows, we will first determine the theoretical relation between the electrostatic force and the external electrolyte, and then simulate the two typical experimental situations shown in Fig. 4 based on this relation of electrostatic repulsion and the mechanical-electrochemical coupling theory described in Section 2.

The electrostatic repulsive force between the indenter and the cell depends on the electrochemical property of the polysaccharide polymer layer and is regulated by the electrolyte environment. It originates from a double electric layer with a characteristic thickness, referred to as the Debye length (λ_D), near the interface between the capsule and the external solution. When the negatively charged AFM tip approaches the capsule, it is subjected to an increasing repulsive electrostatic force (also called as the double-layer force) induced by the double electric layer (Gaboriaud et al., 2008; Mueller et al., 1999; Rijnaarts et al., 1999). The Debye length λ_D for Milli-Q water is ~ 100 nm (Carambassis et al., 1998), whereas in the 100 mM $CaCl_2$ solution, it is as small as ~ 0.55 nm (Israelachvili, 2015). Due to the nature of electrostatic interaction, the double-layer force is obvious in Milli-Q water but negligible in $CaCl_2$ solution. This helps understand the difference in the nanoindentation responses in Stage I under diverse electrolyte conditions in our experimental results, as shown in Fig. 4.

The electrostatic force between the AFM tip and the bacterial cell depends on the

ionic concentrations and the surface charge densities on the bacterial surface and the AFM tip. Since the bacterial size is much larger than the probe, we simplify the electrostatic repulsion as an interaction between the small spherical surface of the tip and a semi-finite plane (Fig. 5(a)). Applying the Derjaguin approximation, we calculate the electrostatic force by (Israelachvili, 2015)

$$F_e = \frac{R_t Z}{\lambda_D} \exp\left(-\frac{h}{\lambda_D}\right), \tag{20}$$

where R_t is the curvature radius of the AFM tip, $Z = 4\pi\omega_c\omega_t\lambda_D^2/\varepsilon$ is the interaction constant. Here, ω_c and ω_t denote the surface charge densities on the capsule and the AFM tip, respectively, and h is the distance between the two surfaces. Therefore, the electrostatic force decays exponentially with the distance with a characteristic decay length, which is taken as the Debye length, λ_D.

It is known from Eq. (20) that the electrostatic force between the indenter and the bacterial cell depends on the curvature radius R_t of the AFM tip, the Debye length λ_D, and the surface charge densities ω_c and ω_t on the capsule and the AFM tip. In the experiments, we adopt an AFM probe with radius of curvature 20 nm and cone angle of 15°. λ_D and ω_t in Milli-Q water are taken to be 100 nm and –0.032 C m^{-2}, respectively (Mueller et al., 1999; Wang et al., 2013). By fitting the experimental data with Eq. (20), the surface charge density on the capsule is found to be $\omega_c = -2\times10^{-4}$ C m^{-2}. As can be seen from the comparison in Fig. 5(b), the theoretical result agrees well with the experimental curve.

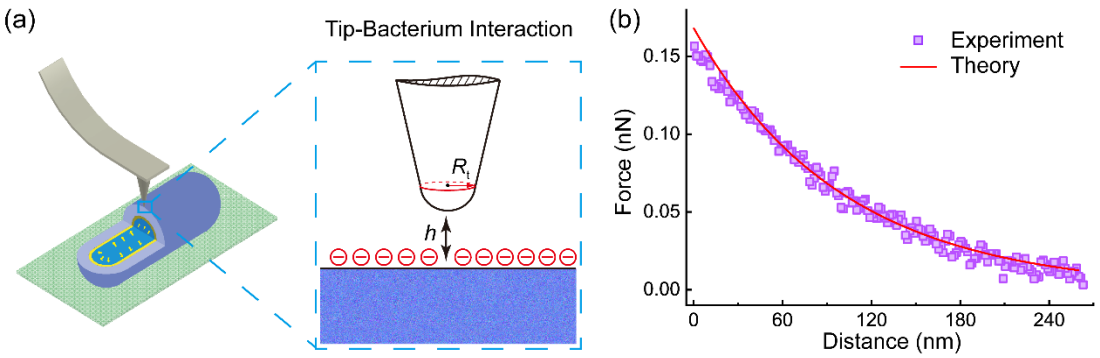

Fig. 5. Electrostatic interaction during the nanoindentation of a bacterial cell. (a) Theoretical model for calculating the electrostatic interaction between the spherical surface of the AFM tip and a semi-infinite plane. (b) Comparison between the theoretical and experimental results for the electrostatic force between the AFM tip and a wild-type bacterial cell in Milli-Q water.

4.2. Numerical simulations of AFM nanoindentation

Now, we simulate the indentation force–depth curves of bacterial cells in the two electrolyte situations shown in Fig. 4 to validate the mechanical-electrochemical coupling theory described in Section 2. In the FEM model, the AFM probe is pressed into the bacterial cell at several points along the cell apex. Based on the transmission electron microscopy images of wild-type *K. pneumoniae* cells (Mularski et al., 2017), the bacterium is modeled as an envelope–capsule bilayer tube. In the contact zone between the bacterial cell and the substrate, the capsule is involved in forming an adhesion layer between the capsule and the substrate (Burks et al., 2003). Thus, we regard the capsule layer in contact with the substrate as a fixed constraint of the displacements along $x = 0$. We assume that no relative displacement exists between the capsule and the envelope (no-slip condition), and the connections of different layers are set to be perfectly bonded. The envelope and the capsule were discretized into eight-node plane-strain hybrid elements (CPE8H).

In the simulations, the deformation of the bacterial cell is decomposed into two parts, which are induced by constrained expansion and indentation, respectively. When

the turgor pressure and external electrolyte are added, the cell swells and reaches the state of mechanical equilibrium. As the AFM tip presses into the cell, the capsule and cell envelope deform successively, as a typical example of the FEM simulation shown in Fig. 6(a). The indentation response in Stage II is controlled mainly by the compression resistance of the capsule. Our detailed analysis, see Eq. (27) in Section 4.3, shows that the compressive resistance depends on the ionic concentration c_0 in the external solution, the number density N of polysaccharide chains, the concentration C_0 of fixed charges, the charge z_0 of a polysaccharide molecule, and the dimensionless parameter ζ of the enthalpy of mixing. The values of C_0, ζ and z_0 are taken according to previous references (Gaboriaud et al., 2008; Xue et al., 2017), and c_0 is obtained in our experiments. However, the polysaccharide chain density N and the thickness t_c of the capsule are difficult to measure directly and, thus, estimated from the indentation curves (Fig. 4).

When the indentation enters Stage III, the force–depth curve becomes approximately linear due to the high elastic stiffness of the cell envelope and the turgor pressure. From the experimental results, we obtain the indentation stiffness as 0.074 N m^{-1} in Milli-Q water and 0.082 N m^{-1} in 100 mM $CaCl_2$. In our previous work (Zhang et al., 2021), we proposed a nanoindentation method to simultaneously measure the turgor pressure p and the Young's modulus E_e of the cell envelope of a live bacterium. Using that method, we determine $p = 80\,\mathrm{kPa}$ and $E_e = 115\,\mathrm{MPa}$. Besides, we take the bacterial radius $R = 350\,\mathrm{nm}$, and the cell envelope thickness $t_e = 26\,\mathrm{nm}$, following Mularski et al. (2017).

In line with our experiments, the normalized concentrations are set as $\nu_w c_0 = 1\times10^{-6}$ in Milli-Q water and $\nu_w c_0 = 2\times10^{-3}$ in 100 mM $CaCl_2$ solution. In the FEM simulations, the thickness of the capsule is estimated as t_e=320 nm in the Mill-

Q water and t_e =152 nm in 100 mM $CaCl_2$ solution, and the number density of polysaccharide chains is estimated as N=2.6×10^{23} m^{-3}. As can be seen from Figs. 6(b) and (c), our numerical simulations based on the proposed mechanical–electrochemical theory are in agreement with the nanoindentation test results. Since the exact values of some parameters used in the simulations, such as the number density N of polysaccharide chains and the capsule thickness t_c, are difficult to measure, the simulation results may have small deviations. Due to the individualism of bacterial cells, the bacterial nanoindentation responses also exhbit distinct dispersion. Our experiments evidence that the thickness of the capsule alters in response to the ionic concentration. Besides, Mei et al. (2006) found that the bacterial polysaccharide capsule may collapse into a more densely packed structure through counterion condensation, and thus its compression resistance may alter as the molecular density of the capsule changes. These detailed mechanisms have not been considered in our simulations

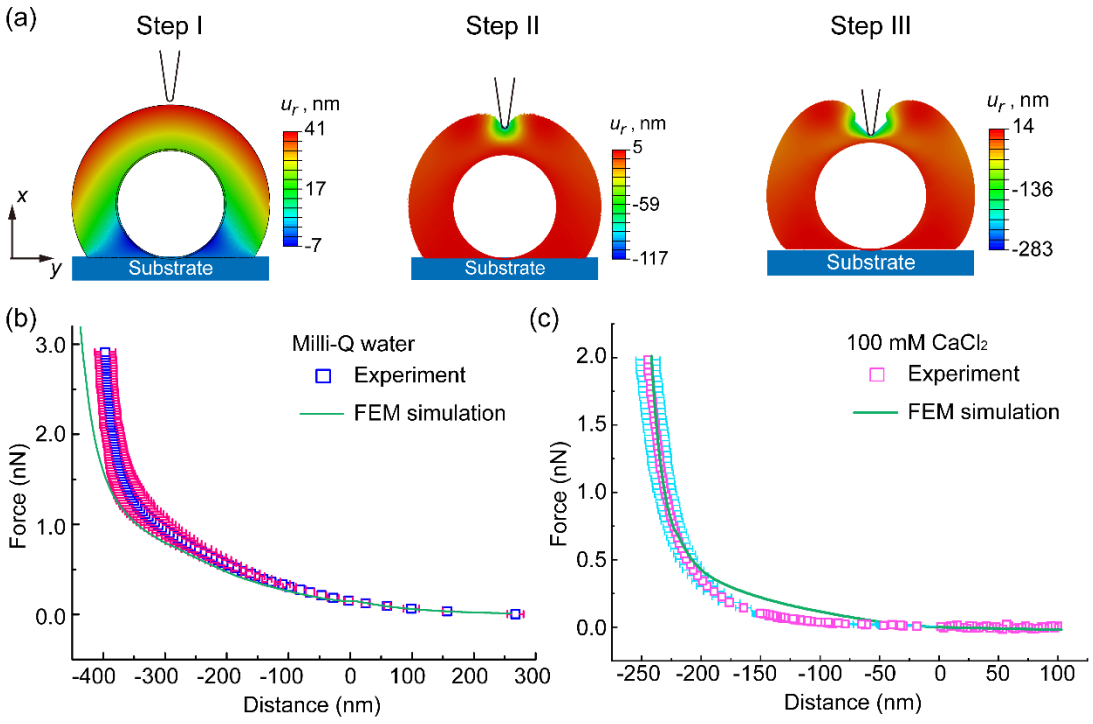

Fig. 6. FEM simulation for the nanomechanical response of a bacterial cell. (a) A numerical model is established to calculate the three-stage deformation behavior of a

cell under external osmotic situation and AFM indentation, where the normalized concentrations $v_w c_0 = 1\times10^{-4}$ and the capsule thickness $t_c = 280\,\text{nm}$. The color represents the radial displacement. Comparison between the numerical and experimental results for the force–depth curves of wild-type bacterial cells (b) in Milli-Q water and (c) in 100 mM $CaCl_2$ solution.

4.3. Compression resistance of polysaccharide capsule

As another application of the mechanical–electrochemical theory for the polysaccharide capsule in Section 2, we further analyze the compression resistance of the polysaccharide capsule of a bacterial cell. The polymeric capsule possesses electrochemical features to sense the electrolyte environment and regulate its compression resistance. We will derive the compressive stress–strain relation and investigate the effect of mechanical–electrochemical coupling mechanisms.

Consider a cylindrical and freely swelling capsule placed in an electrolyte solution and subjected to uniaxial compression in the vertical direction by a permeable platen, as shown in Fig. 7(a). In this case, the capsule can maintain chemical equilibrium with the aid of the external physiological salt solution. Because the double electric layer primarily influences the interfacial interaction and has little effect on the swelling of a bacterial cell, we assume that the electric potential in the freely swelling capsule is homogeneous. Thus, its Cauchy stress is expressed as

$$\boldsymbol{\sigma} = \frac{Nk_{\mathrm{B}}T}{J}\left(\mathbf{F}\cdot\mathbf{F}^{\mathrm{T}} - \mathbf{I}\right) - \Lambda\mathbf{I}\,. \tag{21}$$

The compressive stress between the permeable platen and the capsule contains two parts, $\sigma_c = \sigma_1 + p$, where σ_1 is the Cauchy stress in the vertical direction and p is the fluid pressure, which is generally small and can be neglected. Using Eq. (21), we have

$$\sigma_c = \frac{Nk_{\mathrm{B}}T}{\lambda_1\lambda_2\lambda_3}\left(\lambda_1^2 - 1\right) - \Pi\,, \tag{22}$$

where the stretch ratios $\lambda_i\,(i=1,2,3)$ in the three principal directions of the capsule are

$$\lambda_1=\lambda_0\left(1+\varepsilon_{\mathrm{c}}\right),\quad \lambda_2=\lambda_3=\lambda\,, \tag{23}$$

respectively, where ε_{c} is the normal compressive strain, λ_0 is the stretch ratio of the freely swelling capsule, and λ is the stretch ratio in the lateral direction. To derive the compressive stress–strain relation, we first need to determine the two stretching ratios, λ_0 and λ. Only their analytical expressions are given below, and the detailed derivations are given in Appendix II.

First, the stretch ratio λ_0 in the free swelling capsule is homogeneous and expressed as

$$\begin{aligned} Nk_{\mathrm{B}}T\left(\lambda_0^{-1}-\lambda_0^{-3}\right)=&-\frac{k_{\mathrm{B}}T}{v_{\mathrm{w}}}\left[\ln\left(1-\lambda_0^{-3}\right)+\lambda_0^{-3}+\zeta\lambda_0^{-6}\right]\\ &+k_{\mathrm{B}}T\left[\sqrt{\left(\frac{z_0C_0}{\lambda_0^3-1}\right)^2+4c_0^2}-2c_0\right], \end{aligned} \tag{24}$$

where c_0 is the ionic concentration in the external solution.

The stretch ratio in the lateral direction, λ, can be determined from the equilibrium condition of Cauchy stress $\sigma_2=-p$. It is given by

$$\frac{Nk_{\mathrm{B}}T}{\lambda_1\lambda^2}\left(\lambda^2-1\right)=\Pi\,. \tag{25}$$

In the case of uniaxial compression, the osmotic pressure is obtained from Eqs. (A.21) and (A.23) as

$$\Pi=-\frac{k_{\mathrm{B}}T}{v_{\mathrm{w}}}\left[\ln\left(\frac{J-1}{J}\right)+\frac{1}{J}+\frac{\zeta}{J^2}\right]+k_{\mathrm{B}}T\left[\sqrt{\left(\frac{z_0C_0}{J-1}\right)^2+4c_0^2}-2c_0\right], \tag{26}$$

where $J=\lambda_1\lambda^2$. Thus, we can determine the stretch ratio λ from Eqs. (25) and (26).

Combining Eq. (24) with (26), the compressive stress σ_{c} is related to the stretch

ratio λ_1 by

$$\sigma_c = \frac{Nk_BT}{\lambda_1\lambda^2}\left(\lambda_1^2-1\right)+\frac{k_BT}{v_w}\left[\ln\left(1-\frac{1}{\lambda_1\lambda^2}\right)+\frac{1}{\lambda_1\lambda^2}+\frac{\zeta}{\lambda_1^2\lambda^4}\right] - k_BT\left[\sqrt{\left(\frac{z_0C_0}{\lambda_1\lambda^2-1}\right)^2+4c_0^2}-2c_0\right], \tag{27}$$

where the first term is the stress σ_e induced by the deformation of the polymeric network.

For convenience, let $|\sigma_c|$ and $|\varepsilon_c|$ denote the magnitudes of the applied compressive stress and strain, respectively. With the swelling of the capsule, the PMs are stretched. As the compressive strain $|\varepsilon_c|$ increases, the swelling-induced deformation in the vertical direction is offset, and the polymeric stress σ_e decreases, as shown in Fig. 7(b). However, the PMs in the capsule attract water molecules through osmosis, generating larger polysaccharide–water aggregates, which will be trapped by the PM network. The trapped water endows the capsule with high compression resistance. Thus, the osmotic pressure Π primarily contributes to the compression resistance of the capsule, as shown in Fig. 7(b).

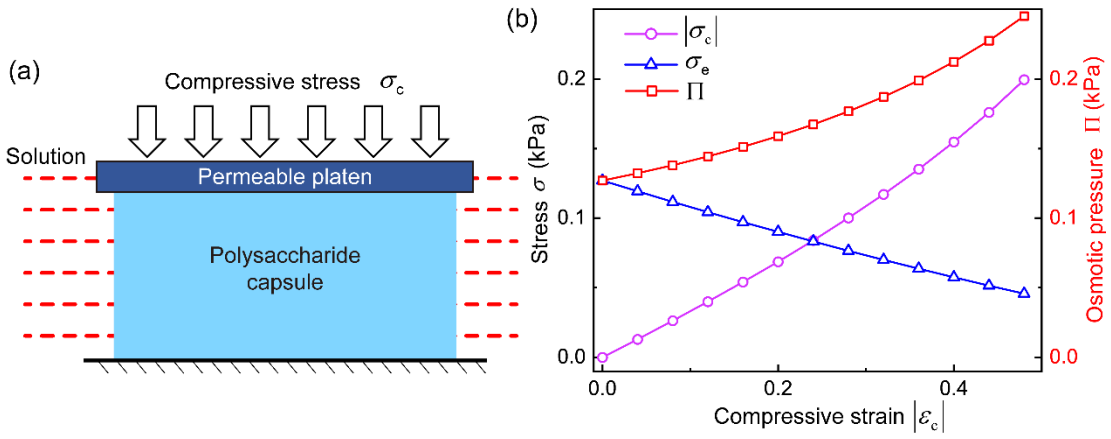

Fig. 7. Uniaxial compression of a polysaccharide capsule in an external solution. (a) Schematic diagram of uniaxial compression. (b) Theoretical results for the variations in

the compressive stress $|\sigma_c|$, polymeric stress σ_e, and osmotic pressure Π with the increase in the compressive strain $|\varepsilon_c|$, which are calculated from Eq. (27).

As can be seen from the compressive stress–strain relation of the capsule in Fig. 8(a), the stress $|\sigma_c|$ is approximately linear with the strain $|\varepsilon_c|$ under a given ionic concentration c_0. The slope of the stress–strain relation is defined as an equivalent compressive modulus $E_c = \Delta\sigma_c / \Delta\varepsilon_c$ to characterize the compression resistance. The higher the ionic concentration c_0, the larger E_c. Furthermore, Fig. 8(b) shows that E_c first increases approximately linearly with $\log(c_0)$ when c_0 is relatively small and finally it approaches a constant of about 0.4 kPa, when $c_0 > 10$ mM. The theory of polysaccharide capsule in Section 2 can be used to reveal the key factors that govern the compression resistance. In the capsule consisting of the polymer macromolecule network embedded in the solution, the free energy is a function of the molar concentration of the solvent, as given in Eqs. (9) and (10). Our theory predicts that under a specified strain of $|\varepsilon_c| = 0.4$, for example, both the compressive stress $|\sigma_c|$ and the osmotic pressure Π increase with the increase in the ionic concentration c_0, while the polymeric stress σ_e is much smaller than Π and thus negligible, as shown in Fig. 8(c). Therefore, the osmosis mainly dictates the compression resistance, originating from two parts: the mixing of PMs and the solvent, and the ionic misbalance in the capsule and the external solution, as expressed in Eqs. (A.19) and (A.20). The theoretical results in Fig. 8(d) demonstrate that the ionic osmotic pressure Π_{ion} is dominant in the osmosis and increases linearly with $\log(c_0)$ when the ionic concentration c_0 is lower than 1.0 mM, while the polymeric osmotic pressure Π_{pol}

is dominant in the osmosis and follows a similar rule when $c_0 > 1.0$ mM. Both the ionic and polymeric osmotic pressures approach constant when $c_0 > 10$ mM. The above analysis demonstrates the significance of mechanical–electrochemical coupling mechanisms in the mechanical resistance of the polysaccharide capsules of bacterial cells.

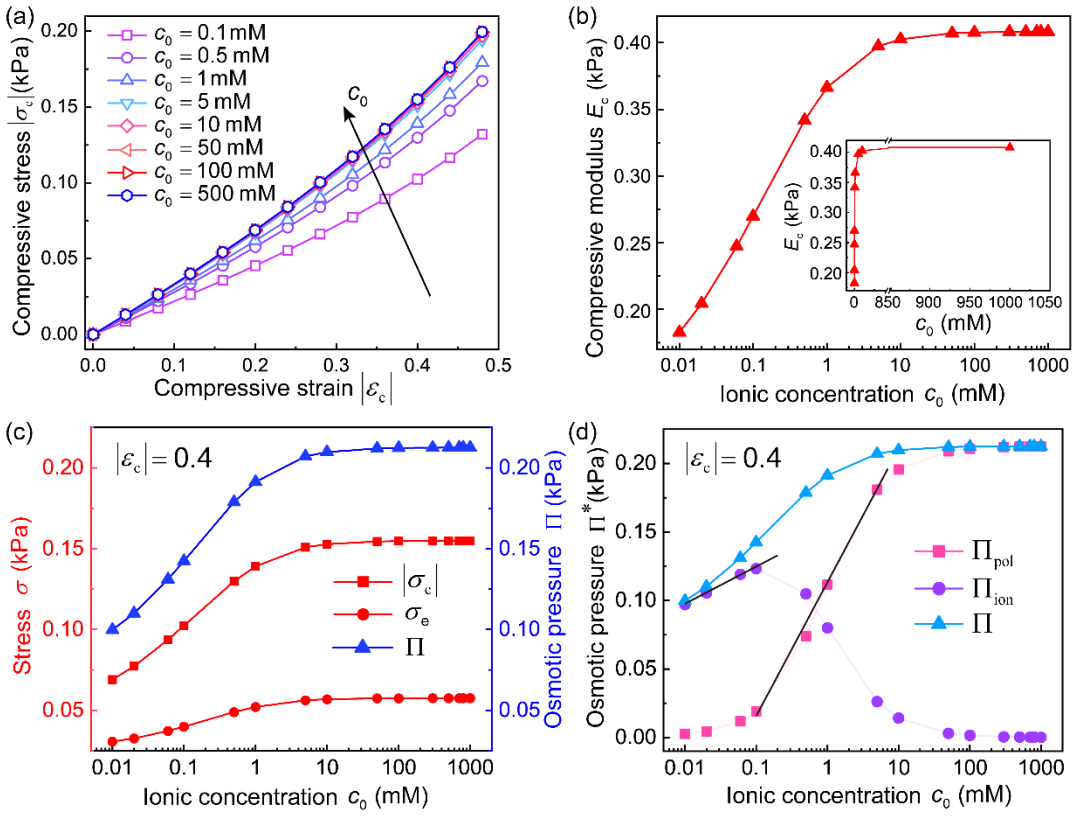

Fig. 8. Theoretical prediction on the compression resistance of a capsule. (a) Compressive stress–strain curves and (b) compressive moduli E_c under different values of the ionic concentration c_0. (c) The variations in the compressive stress $|\sigma_c|$, polymeric stress σ_e, and osmotic pressure Π with respect to the ionic concentration c_0. (d) The variations in the osmotic pressures, including the total osmotic pressure Π, the ionic osmotic pressure Π_{ion}, and the polymeric osmotic pressure Π_{pol}, with

respect to the ionic concentration c_0. The black lines depict that the osmotic pressures increase linearly with $\log(c_0)$.

5. Conclusions

In summary, we have established a mechanical–electrochemical model to investigate the deformation behaviors of bacterial cells. By comparing it with our experiments, we demonstrate that this theory can well interpret the coupled mechanical and electrochemical mechanisms underlying the three-stage nanoindentation response of wild-type *K. pneumoniae* cells under different electrolyte conditions. It is revealed that the electrostatic double-layer force between the bacterium and the AFM tip, which depends on the electrolyte concentration, plays a significant role in the first stage of nanoindentation, while the mechanical and electrochemical properties of the polysaccharide capsule and the mechanics of the cell envelope dominate the second and third stages. Furthermore, we use the proposed model to examine the regulatory role of electrolyte concentration on the stress–strain relation of the polysaccharide capsule of a bacterial cell under uniaxial compression. The results show that the present theory can also be applied to investigate the mechanical and electrochemical buffering effect of the capsule on the osmotic adaptation and to characterize the mechanical properties of diverse bacterial cells. The results obtained from this work can deepen our understanding of the mechanical–electrochemical properties of bacterial cells, and the developed analytical approach can be used to study some bacteria-related medical issues.

CRediT authorship contribution statement

Huanxin Zhang: Established the theoretical model and performed the numerical simulations. **Huabin Wang:** Performed the nanoindentation experiments. **Yuan Gao:** Performed the compression resistance analysis. **Kaixuan Zhang:** Performed the analysis of the experimental data. **Dominic Vella:** Participated in the theoretical analysis and discussion. **Xi-Qiao Feng:** Conceived the problem and designed the study. All authors wrote the paper.

Declaration of competing interest

The authors declare that they have no known competing financial interests or personal relationships that could have appeared to influence the work reported in this paper.

Acknowledgments

This work was supported by the National Natural Science Foundation of China (Grant Nos. 12032014, 11921002, and 11620101001). K. Zhang acknowledges China Postdoctoral Science Foundation (2020M680525).

Appendix I. Implementation of the mechanical–electrochemical model into FEM

To demonstrate the present theory via numerical simulations, we implement the proposed theory into the commercial software *Abaqus 6.14*. Eq. (15) shows the stress field in the capsule depends on three fields, $\mathbf{F}$, $C_\alpha(\mathbf{X})$, and $\hat{\mathbf{D}}(\mathbf{X})$. For illustration, we only consider two species of ions with concentrations C_+ and C_- in the external solution and the capsule. To easily implement the theory into FEM, we perform a Legendre transformation to transform the free energy function w into $\hat{w}$ (Hong et al., 2009; Marcombe et al., 2010; Toh et al., 2014):

$$\hat{w} = w - \left(\mu_+ - e\Phi\right)C_+ - \left(\mu_- + e\Phi\right)C_- - \mu_{\mathrm{w}}C_{\mathrm{w}} - \hat{\mathbf{E}}^{\mathrm{T}}\cdot\hat{\mathbf{D}}. \tag{A.1}$$

Here, the condition of molecular incompressibility is guaranteed by substituting Eq. (13) into the Helmholtz free energy function density Eq. (7), without introducing the Lagrange multiplier Λ.

Let c_0 denote the true concentration of the ions in the external solution. Using Eq. (17), the chemical potential in the external solution can be given by

$$\mu_+ = e\Phi_{\mathrm{e}} + k_{\mathrm{B}}T\ln\left(\frac{c_0}{c_+^{\mathrm{ref}}}\right), \tag{A.2}$$

$$\mu_- = -e\Phi_{\mathrm{e}} + k_{\mathrm{B}}T\ln\left(\frac{c_0}{c_-^{\mathrm{ref}}}\right), \tag{A.3}$$

where Φ_{e} is the electric potential in the external solution.

The ionic equilibrium condition requires that the electrochemical potential in the capsule is equal to that in the external solution. Thus, we have

$$e\left(\Phi - \Phi_{\mathrm{e}}\right) + k_{\mathrm{B}}T\ln\left[\frac{C_+}{\left(J-1\right)c_0}\right] = 0, \tag{A.4}$$

$$e\left(\Phi - \Phi_{\mathrm{e}}\right) + k_{\mathrm{B}}T\ln\left[\frac{\left(J-1\right)c_0}{C_-}\right] = 0. \tag{A.5}$$

Then, the condition of ionic equilibrium is written as

$$\frac{(J-1)c_0}{C_-}=\frac{C_+}{(J-1)c_0}. \tag{A.6}$$

Because the double electric layer has less effect on the swelling of a bacterial cell, we assume that the electric potential in the polysaccharide capsule is uniform, $\partial\Phi/\partial\mathbf{X}=0$, and that the capsule is electroneutral. Thus, Eqs. (1) and (A.1) reduce to

$$z_0C_0-C_-+C_+=0, \tag{A.7}$$

$$\hat{w}=w_{\mathrm{n}}+w_{\mathrm{s}}+w_{\mathrm{i}}-k_{\mathrm{B}}TC_+\ln\left(\frac{C_+}{v_{\mathrm{w}}C_{\mathrm{w}}c_+^{\mathrm{ref}}}\right)-k_{\mathrm{B}}TC_-\ln\left(\frac{C_-}{v_{\mathrm{w}}C_{\mathrm{w}}c_-^{\mathrm{ref}}}\right)-\mu_{\mathrm{w}}C_{\mathrm{w}}. \tag{A.8}$$

Then C_+ and C_- can be solved from Eqs. (A.6) and (A.7) as

$$C_-=\frac{1}{2}\left(\sqrt{4c_0^2(J-1)^2+(z_0C_0)^2}+z_0C_0\right), \tag{A.9}$$

$$C_+=\frac{1}{2}\left(\sqrt{4c_0^2(J-1)^2+(z_0C_0)^2}-z_0C_0\right). \tag{A.10}$$

Consequently, $\hat{w}$ can be expressed as a function of the deformation gradient, the ionic concentration in the external solution, and the fixed charge density on the capsule, i.e., $\hat{w}(\mathbf{F},c_0,C_0)$. When a bacterial cell immersed in a solution reaches the state of electrochemical equilibrium, the ionic concentration in the external solution and the charges fixed in the capsule change little with the swelling of the capsule. Substituting the free energy function $\hat{w}(\mathbf{F},c_0,C_0)$ into (3) gives

$$\boldsymbol{\sigma}=J^{-1}\mathbf{F}\cdot\frac{\partial\hat{w}(\mathbf{F},c_0,C_0)}{\partial\mathbf{F}}. \tag{A.11}$$

The constitutive equation in Eq. (A.11) takes the same form as that of a hyperelastic solid, and the free energy density $\hat{w}(\mathbf{F},c_0,C_0)$ depends mainly on the deformation gradient when the electrolyte concentration is fixed. Therefore, the above theory can be readily implemented in the finite element software, *Abaqus*, by coding the free energy density $\hat{w}$ into the user-defined subroutine, UHYPER.

We first choose a reference state at which the ionic concentration c_0 in the capsule is in an equilibrium state and no mechanical load is applied (Hong et al., 2009).

Let λ_0 denote the isotropic and free-swelling stretch ratio of the PM network, which obeys the relation $\partial\hat{w}/\partial\mathbf{F}=0$. The free-swelling state is characterized by the deformation gradient, $\mathbf{F}_0=\mathrm{diag}\left(\lambda_0,\lambda_0,\lambda_0\right)$. During loading, the deformation gradient $\mathbf{F}$ can be decomposed as

$$\mathbf{F}=\mathbf{F}_\mathrm{e}\cdot\mathbf{F}_0, \tag{A.12}$$

where $\mathbf{F}_\mathrm{e}$ is the deformation gradient in the current configuration with respect to the free-swelling state. Then the free-energy density in Eq. (A. 8) can be rewritten as

$$\hat{w}_\mathrm{e}\left(\mathbf{F}_\mathrm{e},c_0,C_0\right)=\lambda_0^{-3}\hat{w}\left(\mathbf{F},c_0,C_0\right). \tag{A.13}$$

In addition, it is worth mentioning that the ionic concentration in the external solution can be mimicked by a temperature-like variable.

Appendix II. Stretch ratio in a free-swelling capsule

In the considered problem of the capsule under compression, both the fluid phase in the external solution and the capsule of the bacterial cell contain water and free ions. For simplicity, we consider two species of free ions, which carry positive charges and negative charges, respectively. When the system has reached the equilibrium state, the fluid phase uniformly distributed in the capsule, and we have $\sigma_0=-p$. From Eq. (25), we give

$$\Lambda=Nk_\mathrm{B}T\left(\lambda_0^{-1}-\lambda_0^{-3}\right)+p. \tag{A.14}$$

The electrochemical potentials of water and solute in the external solution can be written as (Xue et al., 2017)

$$\mu_\mathrm{w}^\mathrm{ex}=v_\mathrm{w}\left(p-k_\mathrm{B}T\sum_m\overline{c}_m\right), \tag{A.15}$$

$$\mu_m^\mathrm{ex}=k_\mathrm{B}T\ln\frac{\overline{c}_m}{c_m^\mathrm{ref}}, \tag{A.16}$$

where $\overline{c}_m$ is the concentration of free ions *m* in the external solution. *m* can be either

"+" or "–", representing the positive and negative free ions, respectively.

At a quasi-equilibrium state, the electrochemical potentials of fluid phases in the capsule and the external solution are uniform, that is, $\mu_{\mathrm{w}} = \mu_{\mathrm{w}}^{\mathrm{ex}}$ and $\mu_m = \mu_m^{\mathrm{ex}}$. From Eqs. (16) and (17), Λ and C_m are derived as

$$\begin{aligned}\Lambda = &-\frac{k_{\mathrm{B}}T}{v_{\mathrm{w}}}\left[\ln\left(\frac{v_{\mathrm{w}}C_{\mathrm{w}}}{1+v_{\mathrm{w}}C_{\mathrm{w}}}\right)+\frac{1}{1+v_{\mathrm{w}}C_{\mathrm{w}}}+\frac{\zeta}{\left(1+v_{\mathrm{w}}C_{\mathrm{w}}\right)^2}\right]\\ &+k_{\mathrm{B}}T\sum_m\left(\frac{C_m}{v_{\mathrm{w}}C_{\mathrm{w}}}-\bar{c}_m\right)+p,\end{aligned} \tag{A.17}$$

$$C_m = v_{\mathrm{w}}C_{\mathrm{w}}\bar{c}_m \exp\left(-\frac{e\Phi z_m + \Lambda v_m}{k_{\mathrm{B}}T}\right). \tag{A.18}$$

According to Eq. (A.14), the osmosis of the capsule affects the contractility of the PM network, and the osmotic pressure is expressed as $\Pi = Nk_{\mathrm{B}}T\left(\lambda_0^{-1}-\lambda_0^{-3}\right)$. It can be divided into two parts: the polymeric osmotic pressure Π_{pol} arising from the mixing of PMs and water, and the ionic osmotic pressure Π_{ion} due to the misbalance of ions in the capsule and the external solution. They are written as

$$\Pi_{\mathrm{pol}} = -\frac{k_{\mathrm{B}}T}{v_{\mathrm{w}}}\left[\ln\left(\frac{v_{\mathrm{w}}C_{\mathrm{w}}}{1+v_{\mathrm{w}}C_{\mathrm{w}}}\right)+\frac{1}{1+v_{\mathrm{w}}C_{\mathrm{w}}}+\frac{\zeta}{\left(1+v_{\mathrm{w}}C_{\mathrm{w}}\right)^2}\right], \tag{A.19}$$

$$\Pi_{\mathrm{ion}} = k_{\mathrm{B}}T\sum_m\left(\frac{C_m}{v_{\mathrm{w}}C_{\mathrm{w}}}-\bar{c}_m\right). \tag{A.20}$$

Since the concentration of the solutes is small, we ignore the contribution of the solutes to the incompressibility condition in Eq. (13), i.e., $1+v_{\mathrm{w}}C_{\mathrm{w}} = J$. Thus, the polymeric osmotic pressure is given by

$$\Pi_{\mathrm{pol}} = -\frac{k_B T}{v_{\mathrm{w}}}\left[\ln\left(\frac{J-1}{J}\right)+\frac{1}{J}+\frac{\zeta}{J^2}\right]. \tag{A.21}$$

In the external solution, both the concentrations of negative and positive ions are set as c_0, that is, $\bar{c}_m = c_0$. In addition, the effect of Λv_m on the electric potentials of

ions is in general negligible. By using Eq. (A.18), $C_+C_- = \left(v_{\mathrm{w}}C_{\mathrm{w}}c_0\right)^2$ and the electroneutrality $C_+ - C_- + z_0C_0 = 0$, we obtain

$$C_\pm = \frac{1}{2}\left[\mp z_0C_0 + \sqrt{\left(z_0C_0\right)^2 + 4\left(v_{\mathrm{w}}C_{\mathrm{w}}c_0\right)^2}\right]. \tag{A.22}$$

Thus Π_{ion} is recast as

$$\Pi_{\mathrm{ion}} = k_BT\left[\sqrt{\left(\frac{z_0C_0}{J-1}\right)^2 + 4c_0^2} - 2c_0\right]. \tag{A.23}$$

From Eqs. (A.14), (A.17), (A.21), and (A.23), it is known that the stretch ratio λ_0 of the free swelling capsule can be determined from

$$\begin{aligned} Nk_{\mathrm{B}}T\left(\lambda_0^{-1} - \lambda_0^{-3}\right) = &-\frac{k_{\mathrm{B}}T}{v_{\mathrm{w}}}\left[\ln\left(1-\lambda_0^{-3}\right) + \lambda_0^{-3} + \zeta\lambda_0^{-6}\right] \\ &+ k_{\mathrm{B}}T\left[\sqrt{\left(\frac{z_0C_0}{\lambda_0^3-1}\right)^2 + 4c_0^2} - 2c_0\right]. \end{aligned} \tag{A.24}$$

References

Abraham, T., Giasson, S., Gohy, J.F., Jerome, R., 2000. Direct measurements of interactions between hydrophobically anchored strongly charged polyelectrolyte brushes. Langmuir 16, 4286–4292.

Arnoldi, M., Fritz, M., Bauerlein, E., Radmacher, M., Sackmann, E., Boulbitch, A., 2000. Bacterial turgor pressure can be measured by atomic force microscopy. Phys. Rev. E 62, 1034–1044.

Boulbitch, A., Quinn, B., Pink, D., 2000. Elasticity of the rod-shaped Gram-negative eubacteria. Phys. Rev. Lett. 85, 5246–5249.

Buda, R., Liu, Y., Yang, J., Hegde, S., Stevenson, K., Bai, F., Pilizota, T., 2016. Dynamics ofEscherichia coli's passive response to a sudden decrease in external osmolarity. Proc. Natl. Acad. Sci. U.S.A. 113, 5838–5846.

Burks, G.A., Velegol, S.B., Paramonova, E., Lindenmuth, B.E., Feick, J.D., Logan, B.E., 2003. Macroscopic and nanoscale measurements of the adhesion of bacteria with varying outer layer surface composition. Langmuir 19, 2366–2371.

Camesano, T.A., Logan, B.E., 2000. Probing bacterial electrosteric interactions using atomic force microscopy. Environ. Sci. Technol. 34, 3354–3362.

Carambassis, A., Jonker, L.C., Attard, P., Rutland, M.W., 1998. Forces measured between hydrophobic surfaces due to a submicroscopic bridging bubble. Phys. Rev. Lett. 80, 5357–5360.

Considine, R.F., Drummond, C.J., Dixon, D.R., 2001. Force of interaction between a biocolloid and an inorganic oxide: Complexity of surface deformation, roughness, and brushlike behavior. Langmuir 17, 6325–6335.

Deng, Y., Sun, M., Shaevitz, J.W., 2011. Direct measurement of cell wall stress

stiffening and turgor pressure in live bacterial cells. Phys. Rev. Lett. 107, 158101.

Flory, P.J., 1942. Thermodynamics of high polymer solutions. J. Chem. Phys. 10, 51–61.

Flory, P.J., 1953. Principles of polymer chemistry. Cornell University Press, New York.

Gaboriaud, F., Gee, M.L., Strugnell, R., Duval, J.F.L., 2008. Coupled electrostatic, hydrodynamic, and mechanical properties of bacterial interfaces in aqueous media. Langmuir 24, 10988–10995.

Guo, S., Kwek, M.Y., Toh, Z.Q., Pranantyo, D., Kang, E.-T., Loh, X.J., Zhu, X., Janczewski, D., Neoh, K.G., 2018. Tailoring Polyelectrolyte Architecture To Promote Cell Growth and Inhibit Bacterial Adhesion. ACS. Appl. Mater. Interfaces 10, 7882–7891.

Hammerschmidt, S., Wolff, S., Hocke, A., Rosseau, S., Muller, E., Rohde, M., 2005. Illustration of pneumococcal polysaccharide capsule during adherence and invasion of epithelial cells. Infect. Immun. 73, 4653–4667.

Hayashi, H., Tsuneda, S., Hirata, A., Sasaki, H., 2001. Soft particle analysis of bacterial cells and its interpretation of cell adhesion behaviors in terms of DLVO theory. Colloids. Surf. B Biointerfaces 22, 149–157.

Hong, W., Liu, Z., Suo, Z., 2009. Inhomogeneous swelling of a gel in equilibrium with a solvent and mechanical load. Int. J. Solids Struct. 46, 3282–3289.

Hong, W., Zhao, X., Suo, Z., 2010. Large deformation and electrochemistry of polyelectrolyte gels. J. Mech. Phys. Solids 58, 558–577.

Huggins, M.L., 1942. Some properties of solutions of long-chain compounds. J. Phys. Chem. 46, 151–158.

Hwang, G., Ahn, I.-S., Mhin, B.J., Kim, J.-Y., 2012. Adhesion of nano-sized particles to the surface of bacteria: Mechanistic study with the extended DLVO theory. Colloids. Surf. B Biointerfaces 97, 138–144.

Israelachvili, J.N., 2015. Intermolecular and surface forces. Academic press, California.

James, S.A., Hilal, N., Wright, C.J., 2017. Atomic force microscopy studies of bioprocess engineering surfaces - imaging, interactions and mechanical properties mediating bacterial adhesion. Biotechnol. J. 12, 1600698.

Jenney, A.W., Clements, A., Farn, J.L., Wijburg, O.L., McGlinchey, A., Spelman, D.W., Pitt, T.L., Kaufmann, M.E., Liolios, L., Moloney, M.B., Wesselingh, S.L., Strugnell, R.A., 2006. Seroepidemiology of Klebsiella pneumoniae in an Australian tertiary hospital and its implications for vaccine development. J. Clin. Microbiol. 44, 102–107.

Jiang, H., Sun, S.X., 2010. Morphology, growth, and size Limit of bacterial cells. Phys. Rev. Lett. 105, 028101.

Liu, Y., Li, B., Feng, X.-Q., 2020. Buckling of growing bacterial chains. J. Mech. Phys. Solids 145, 104146.

Marcombe, R., Cai, S., Hong, W., Zhao, X., Lapusta, Y., Suo, Z., 2010. A theory of constrained swelling of a pH-sensitive hydrogel. Soft Matter 6, 784–793.

Mei, Y., Lauterbach, K., Hoffmann, M., Borisov, O.V., Ballauff, M., Jusufi, A., 2006. Collapse of spherical polyelectrolyte brushes in the presence of multivalent counterions. Phys. Rev. Lett. 97, 158301.

Miermont, A., Waharte, F., Hu, S., McClean, M.N., Bottani, S., Leon, S., Hersen, P., 2013. Severe osmotic compression triggers a slowdown of intracellular signaling, which can be explained by molecular crowding. Proc. Natl. Acad. Sci. U.S.A. 110, 5725–5730.

Monteiro, J.M., Fernandes, P.B., Vaz, F., Pereira, A.R., Tavares, A.C., Ferreira, M.T., Pereira, P.M., Veiga, H., Kuru, E., VanNieuwenhze, M.S., Brun, Y.V., Filipe, S.R., Pinho, M.G., 2015. Cell shape dynamics during the staphylococcal cell cycle. Nat. Commun. 6, 8055.

Moxon, E.R., Kroll, J.S., 1990. The role of bacterial polysaccharide capsules as virulence factors. Curr. Top. Microbiol. Immunol. 150, 65–85.

Mueller, D.J., Fotiadis, D., Scheuring, S., Mueller, S.A., Engel, A., 1999. Electrostatically balanced subnanometer imaging of biological specimens by atomic force microscope. Biophys. J. 76, 1101–1111.

Mularski, A., Wilksch, J., Hanssen, E., Li, J., Tomita, T., Pidot, S.J., Stinear, T., Separovic, F., Strugnell, D., 2017. A nanomechanical study of the effects of colistin on the Klebsiella pneumoniae AJ218 capsule. Eur. Biophys. J. Biophys. Lett. 46, 351–361.

Ohyama, T., Mugikura, S., Nishikawa, M., Igarashi, K., Kobayashi, H., 1992. Osmotic adaptation of Escherichia coli with a negligible proton motive force in the presence of carbonyl cyanide m-chlorophenylhydrazone. J. Bacteriol. 174, 2922–2928.

Pelling, A.E., Li, Y.N., Shi, W.Y., Gimzewski, J.K., 2005. Nanoscale visualization and characterization of Myxococcus xanthus cells with atomic force microscopy. Proc. Natl. Acad. Sci. U.S.A. 102, 6484–6489.

Phanphak, S., Georgiades, P., Li, R., King, J., Roberts, I.S., Waigh, T.A., 2019. Super-Resolution Fluorescence Microscopy Study of the Production of K1 Capsules by Escherichia coil: Evidence for the Differential Distribution of the Capsule at the Poles and the Equator of the Cell. Langmuir 35, 5635–5646.

Pilizota, T., Shaevitz, J.W., 2012. Fast, multiphase volume adaptation to hyperosmotic shock by Escherichia coli. Plos One 7, e35205.

Poortinga, A.T., Bos, R., Norde, W., Busscher, H.J., 2002. Electric double layer interactions in bacterial adhesion to surfaces. Surf. Sci. Rep. 47, 3–32.

Rijnaarts, H.H.M., Norde, W., Lyklema, J., Zehnder, A.J.B., 1999. DLVO and steric contributions to bacterial deposition in media of different ionic strengths. Colloids. Surf. B Biointerfaces 14, 179–195.

Rojas, E., Theriot, J.A., Huang, K.C., 2014. Response of Escherichia coli growth rate to osmotic shock. Proc. Natl. Acad. Sci. U.S.A. 111, 7807–7812.

Stokes, J.R., Macakova, L., Chojnicka-Paszun, A., de Kruif, C.G., de Jongh, H.H.J., 2011. Lubrication, Adsorption, and Rheology of Aqueous Polysaccharide Solutions. Langmuir 27, 3474–3484.

Straub, H., Bigger, C.M., Valentin, J., Abt, D., Qin, X.-H., Eberl, L., Maniura-Weber, K., Ren, Q., 2019. Bacterial Adhesion on Soft Materials: Passive Physicochemical Interactions or Active Bacterial Mechanosensing? Adv. Healthc. Mater. 8, 1801323.

Suo, Z., Zhao, X., Greene, W.H., 2008. A nonlinear field theory of deformable dielectrics. J. Mech. Phys. Solids 56, 467–486.

Toh, W., Ng, T.Y., Hu, J., Liu, Z., 2014. Mechanics of inhomogeneous large deformation of photo-thermal sensitive hydrogels. Int. J. Solids Struct. 51, 4440–4451.

Vadillo-Rodriguez, V., Busscher, H.J., Norde, W., de Vries, J., van der Mei, H.C., 2004. Relations between macroscopic and microscopic adhesion of Streptococcus mitis strains to surfaces. Microbiology-Sgm 150, 1015–1022.

Vella, D., Ajdari, A., Vaziri, A., Boudaoud, A., 2012a. Indentation of Ellipsoidal and Cylindrical Elastic Shells. Phys. Rev. Lett. 109, 144302.

Vella, D., Ajdari, A., Vaziri, A., Boudaoud, A., 2012b. The indentation of pressurized elastic shells: from polymeric capsules to yeast cells. J. R. Soc. Interface 9, 448–455.

Wang, H., Wilksch, J.J., Lithgow, T., Strugnell, R.A., Gee, M.L., 2013. Nanomechanics measurements of live bacteria reveal a mechanism for bacterial cell protection: the polysaccharide capsule in Klebsiella is a responsive polymer hydrogel that adapts to osmotic stress. Soft Matter 9, 7560–7567.

Xue, S.-L., Li, B., Feng, X.-Q., Gao, H., 2017. A non-equilibrium thermodynamic model for tumor extracellular matrix with enzymatic degradation. J. Mech. Phys. Solids 104, 32–56.

Zhang, H., Wang, H., Wilksch, J.J., Strugnell, R.A., Gee, M.L., Feng, X.-Q., 2021. Measurement of the interconnected turgor pressure and envelope elasticity of live bacterial cells. Soft matter 17, 2042–2049.

Zhao, X., Hong, W., Suo, Z., 2007. Electromechanical hysteresis and coexistent states in dielectric elastomers. Phys. Rev. B 76, 134113.